Results in Physics 35 (2022) 105290

Contents lists available at ScienceDirect

Results in Physics

journal homepage: www.elsevier.com/locate/rinp

Influence of curvature on the dynamical susceptibility of bent nanotubes

E. Saavedra [a], S. Castillo-Sepúlveda [b,c], R.M. Corona [a,c], D. Altbir [a,c], J. Escrig [a,c,*], V.L. Carvalho-Santos [d]

[a] Universidad de Santiago de Chile, Departamento de Física, Avda. Víctor Jara, 3493, Estación Central, Santiago, Chile
[b] Facultad de Ingeniería, Universidad Autónoma de Chile, Avda. Pedro de Valdivia 425, Providencia, Chile
[c] Center for the Development of Nanoscience and Nanotechnology, Avda. Libertador Bernardo O'Higgins 3363, 9170124 Santiago, Chile
[d] Universidade Federal de Viçosa, Departamento de Física, Avenida Peter Henry Rolfs s/n, 36570-000, Viçosa, MG, Brazil

ARTICLE INFO

Keywords:
Dynamical susceptibility
Magnetic nanotubes
Bent nanotubes
Curvature
Micromagnetic simulations

ABSTRACT

In this work we analyze the influence of curvature on the dynamic properties of the magnetization in bent nanotubes. Our results show that both the resonance frequencies and the number of resonant peaks have a strong dependence on the ground state of the magnetization created by the curvature. Our results can be understood from the analysis of the effective anisotropy and the Dzyaloshinskii–Moriya interaction (DMI) induced by curvature. The ability to control the dynamic properties of these curved ferromagnets makes them excellent candidates for developing applications based on resonant modes of spin waves.

Introduction

Effects induced by geometry on the properties of solid-state systems have been a hot topic in physics [1–3]. In magnetism, curvature-induced effects on the magnetization of systems at the nanoscale are the heart of a new branch in physics known as curvilinear micromagnetism [4–6]. In part, this increasing interest on the interplay between geometry and magnetic phenomena has been fostered by the development of experimental techniques that allow the production and characterization of magnetic nanoparticles with a broad range of shapes and sizes [7,8]. Induction due to curvature of effective interactions such as the exchange-driven anisotropy, Dzyaloshinskii–Moriya interaction (DMI) [9], and the intrinsic DMI-driven anisotropy [10] in magnetic nanoshells confirms that curvature plays a crucial role on the magnetization at the nanoscale. In addition, such effective interactions are responsible for a diversity of new phenomena such as the increase in the skyrmion stabilization in dome-like structures [11–13], the nucleation of a vortex–antivortex pair in shells with variable Gaussian curvature [14,15], and the emergence of weak ferromagnetism in curved antiferromagnets [16], among others.

Interesting evidence of such phenomena appears in low-dimensional systems such as nanowires (NWs) and nanotubes (NTs). Some examples of curvature-induced phenomena are the geometrical barriers in cylindrical [17,18] and rectangular [19] NWs, responsible for the pinning of transverse domain walls (DWs) at specific positions along an NW, where they start to rotate with a frequency dependent on external stimuli. A DW pinning is also observed in bent parabolic NWs due to an exchange-driven effective force originated from the curvature gradient [20]. The introduction of bents in cylindrical NWs and NTs is also responsible for the increasing in the energy of vortex DWs, decreasing their stability and inhibiting the collapse of transverse walls [21]. Additionally, the new freedom degree introduced by bending NWs brings back the Walker breakdown phenomenon [22], where the Walker critical field is a linear function of the bent curvature [23,24]. Moreover, a curvature-induced second critical field in addition to the Walker field was recently predicted in DWs propagating along bent NWs with rectangular cross-section [25].

It is also interesting that the geometry of a nanoparticle influences the high-frequency dynamical magnetic response to external stimuli. For instance, the dynamic susceptibility associated with resonant spin wave resonant modes (SWRM) is strongly affected by both the geometric distribution of a nanoparticle array [26–28] and the nanoparticle geometry [29–32]. In this context, Abeed et al. [33] showed that the inclusion of defects such as holes or hill-like structures in magnetic nanodots is responsible for changes in the SWRM properties. Additionally, the introduction of modulations in NWs yields the appearance of peaks in the SWRM that depend on the geometrical modulation [34–36], and that are not observed in the absence of such modulations. Finally, the geometry of antidots in a ferromagnetic system influences the high-frequency dynamical magnetic response to a magnetic field pulse [37]. Therefore, due to the possibility of controlling the magnetic permeability by tailoring the particle geometry, one can state that curved

* Corresponding author at: Universidad de Santiago de Chile, Departamento de Física, Avda. Víctor Jara, 3493, Estación Central, Santiago, Chile.
E-mail address: juan.escrig@usach.cl (J. Escrig).

https://doi.org/10.1016/j.rinp.2022.105290
Received 10 December 2021; Received in revised form 16 January 2022; Accepted 28 January 2022
Available online 12 February 2022

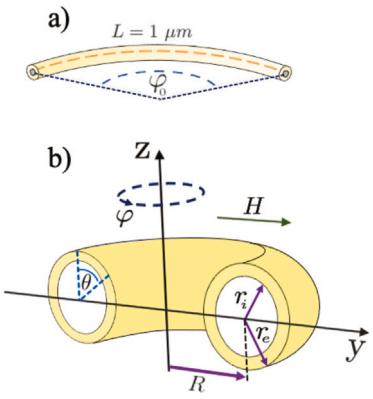

Fig. 1. Geometric parameters of a toroidal geometry describing a bent NT. R and r are the toroidal and poloidal radii, respectively, while φ and θ are the azimuthal and poloidal angles, respectively. Therefore, a nanotube is characterized by an external and internal radius given respectively by r_e and r_i, and a length L.

ferromagnets are good candidates for developing new applications based on microwaves [38].

Based on what is presented above and on the fact that the inclusion of curvature changes several magnetic properties of NWs and NTs, in this work we analyze the dynamical susceptibility of permalloy curved NWs and NTs with circular cross-section. We describe the magnetization dynamics through the potential spectra and the spin wave modes resonance profiles when a time-dependent external magnetic field is applied in the system.

This work is organized as follows: In Section 'Micromagnetic simulations' we introduce the considered magnetic and geometric parameters, as well as the methodology we use to obtain the dynamic susceptibility of these systems. In Section 'Results and discussion' we present our results, including the equilibrium configurations obtained as a function of the curvature of the system and the dynamic susceptibility spectrum for different geometries. Finally, we characterize each of the spatial profiles of the resonance modes. In addition, we briefly discuss our results, suggesting the appearance of effective anisotropy and DMI induced by curvature. In Section 'Conclusions' we present our conclusions.

Micromagnetic simulations

In this work we focus on the dynamical susceptibility of a bent cylindrical NT parameterized as a toroidal section. The geometrical parameters of the considered system are depicted in Fig. 1, where R and r are the toroidal and poloidal radii, respectively, and $\varphi \in [0, \varphi_0]$ and $\theta \in [0, 2\pi]$ are the azimuthal and poloidal angles [39], respectively. Here, φ_0 is the opening angle of the NT so that R and φ_0 are related as $R = L/\varphi_0$. In this work, all considered NTs have a fixed length $L = 1\ \mu$m. The geometrical description of the NT cross-section is given by the external and internal radii, that is, r_e and r_i, respectively. It is convenient to define the ratio $\beta = r_i/r_e$, in such a way that $\beta = 0.0$ represents a solid structure, while $\beta \to 1$ corresponds to a very thin tube. In our calculations we considered a system with a fix external radius $r_e = 25$ nm, and five different values of β (0.0, 0.3, 0.5, 0.7 and 0.8).

We performed micromagnetic simulations using the Object Oriented MicroMagnetic Framework (OOMMF) [40], which uses the Runge–Kutta–Fehlberg method [41,42], within the finite difference approach [43] to integrate the Landau–Lifshitz–Gilbert (LLG) equation [44,45]

$$\frac{d\mathbf{M}}{dt} = -\gamma \mathbf{M} \times \mathbf{H}_{eff} + \frac{\alpha}{M_s} \mathbf{M} \times \frac{d\mathbf{M}}{dt}, \tag{1}$$

where α is the phenomenological damping constant, γ is the gyromagnetic ratio, M_s is the saturation magnetization, and $\mathbf{H}_{eff}$ is the effective magnetic field, originated from exchange, dipolar, and Zeeman interactions. We consider a damping coefficient $\alpha = 0.008$, which is small enough to adequately describe a dynamic study of the magnetization [46–49], and allows to obtain a better resolution of the spin wave modes in the susceptibility spectra. We use cell sizes of $2 \times 2 \times 2$ nm^3, and adopt the typical permalloy material parameters, that is, exchange coupling $A = 13 \times 10^{-12}$ J/m, saturation magnetization $M_s = 860 \times 10^3$ A/m, and vanishing magnetocrystalline anisotropy.

To analyze the frequency spectra of the excited system, we use the Ringdown method [50,51], which consists of two steps: (i) we obtain the minimum energy configuration at zero external field [52]; (ii) we perturb the system from its equilibrium state with a time-dependent field of the form $\mathbf{h}(t) = h_0 \mathrm{Sinc}\left[2\pi f_{\max}(t - t_0)\right] \hat{y}$ [53], where $h_0 = 1$ mT, $f_{\max} = 40$ GHz, and $t_0 = 1$ ns. The amplitude of this pulse should be small enough to ensure that the system response is in the linear regime [37,46,53–55].

The time evolution of the magnetization under the action of the exciting field is collected during 10 ns. The magnetization configuration is recorded at uniform time intervals of 10 ps, which allows to obtain a spectral resolution of 0.1 GHz [56]. The small exciting magnetic field $h(t)$ and the calculated magnetization distribution $M(r, t)$ is transformed into the frequency domain $[h(\omega), M(\omega)]$ using the Fast Fourier Transform (FFT) method. The dynamic susceptibility (DS), which corresponds to the imaginary part of the magnetic susceptibility [57], is calculated by dividing the Fourier transform of the response $M(\omega)$ by the Fourier transform of the excitation $h(\omega)$.

Results and discussion

From the above-described procedure we have obtained the equilibrium magnetization configurations of the bent NT in the absence of external magnetic fields. The obtained results, depicted in Fig. 2, evidence that the magnetic ground state depends on both wall thickness (defined by β) and curvature of the tube (defined by the opening angle φ_0). Due to the in-surface shape anisotropy created by the aspect ratio R/L, in both, the solid NW ($\beta = 0$) and the NT ($\beta > 0$), the ground state consists of a quasi-tangent to the surface magnetization texture in such a way that the minimum energy configuration goes from a quasi-single domain (SD) state for $\varphi_0 = \pi/16$ (straight NW) to a vortex state for $\varphi_0 = 2\pi$ (nanotorus). This result agrees with previously obtained results for straight [58] and bent NTs [59], and nanotori [39,60]. Nevertheless, the dipolar cost associated with magnetostatic surface charges yields the formation of a vortex domain wall at the ends of the thick NTs, which is clearly evidenced for lower values of β. It is worth notice that the obtained equilibrium magnetization configurations in bent NTs do not consist of purely in-surface states due to a curvature-induced exchange-driven effective anisotropy and DMI [9].

After determining the magnetic ground state for the considered bent NTs, we have systematically performed simulations to study the spin wave modes (SWM) of these nanostructures. In this case, we consider a magnetic field pulse applied along the y-direction, which actives SWM along the xz-components of the magnetic moments. Our results evidence that the characteristic frequency and amplitude of the dynamic susceptibility (DS) depend on the NT curvature and thickness. Fig. 3 illustrates our results for NTs with opening angles $\varphi_0 = \pi/16$ (a), $\pi/4$ (b), $\pi/2$ (c), π (d), $3\pi/2$ (e), and 2π (f). Black, red, blue, magenta, and dark yellow lines show respectively the corresponding frequencies for $\beta = 0.0$, 0.3, 0.5, 0.7, and 0.8. These results evidence the appearance of at least six distinct modes, here called modes 1 to 6, each corresponding to a resonant peak shown in Fig. 3. As reported for spherical magnetic nanoparticles [30], the amplitude of the DS and the frequency of the SWM increase as the NT thickness decreases. Nevertheless, the NT curvature affects only the amplitude of the DS, which decreases as the curvature increases. The influence of the curvature on the dynamical

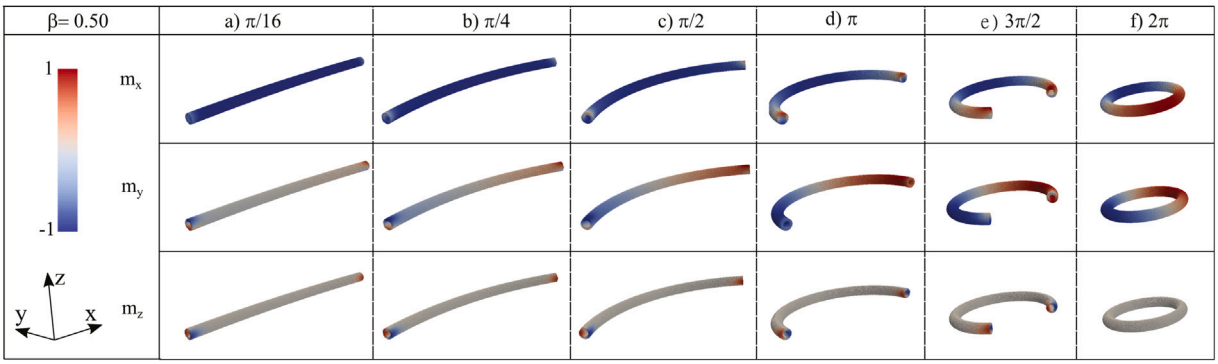

Fig. 2. Equilibrium configurations at zero external field for $\beta = 0.5$ and different bends defined by the poloidal angle φ_0. The color code on the left represents the magnetization along the three coordinate axes. (For interpretation of the references to color in this figure legend, the reader is referred to the web version of this article.)

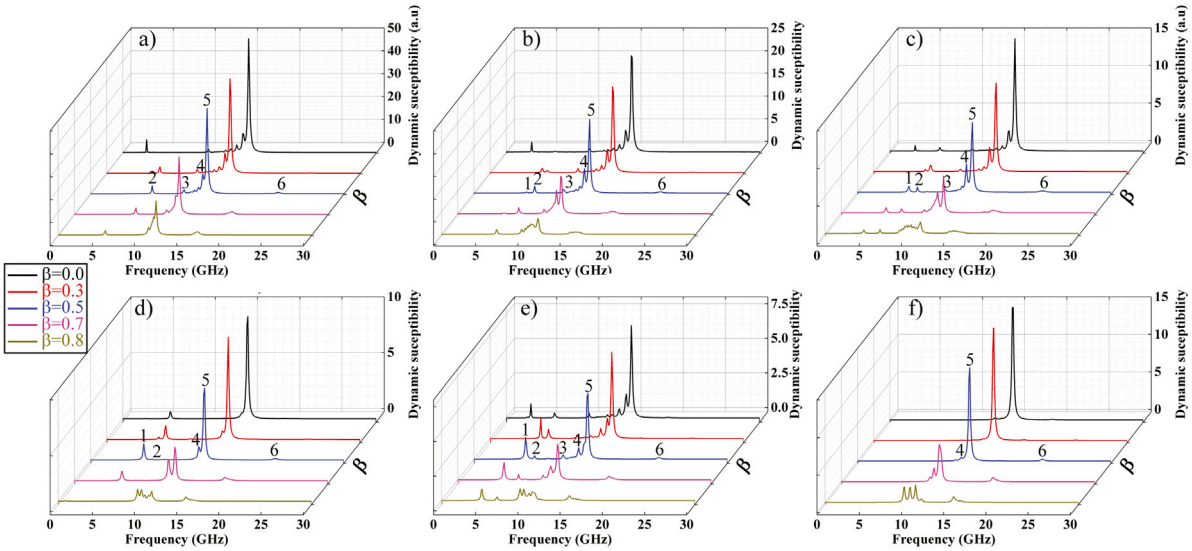

Fig. 3. Dynamic susceptibility spectra for (a) $\varphi_0 = \pi/16$, (b) $\varphi_0 = \pi/4$, (c) $\varphi_0 = \pi/2$, (d) $\varphi_0 = \pi$, (e) $\varphi_0 = 3\pi/2$, (f) $\varphi_0 = 2\pi$.

response of ferromagnetic NTs can be understood from the emergence of exchange-driven effective interactions, as it will be explained later in this text.

To better understand the spatial nature of the SW resonance modes, we obtained from numerical calculations the spatial distribution of the amplitudes corresponding to the spectra of the resonant modes [61,62]. Therefore, we calculated the time Fourier image of each magnetic site $m\,(r_{ijk}, \omega_n) = \mathrm{DFTt}(m(r_{ijk}, t_n))$ (obtained from the OOMMF simulations), where DFTt is the Fourier transform, subscripts ijk correspond to spatial coordinates x, y, and z of each cell, while the subscript n denotes the position of the power spectrum frequency. The Fourier coefficient modulus has information about the amplitude inside the magnetic element.

In Fig. 4 we show the spatial distribution of SWRM for NT with $\beta = 0.5$ and different curvatures. Following the ideas presented previously for straight NTs [34], we can classify the observed modes into three main groups: (a) Low-frequency modes (modes 1 and 2), whose perturbations are mainly due to the magnetization texture at the NT borders; (b) Intermediate frequency modes (mode 3), whose perturbations are mainly due to the ring-shaped magnetization patterns formed near the NT borders; and (c) modes at high frequencies (modes 4, 5 and 6), whose perturbations are mainly localized at the center of the magnetic structures. We can differentiate the high-frequency SWRM by observing the number of antinodes that their resonant profiles present on the surface. In this context, the obtained profile along a central line of the nanostructure evidence that mode 4 has three antinodes, while mode 5 has a single antinode at the NT center. Therefore, mode 5 is the fundamental mode of the NT because its characteristic peak presents the highest amplitude [54]. Finally, mode 6 has two antinodes whose amplitude is smaller than that of mode 5 (see supplementary material Fig. 6). It is worth notice that the obtained results for almost straight NTs $\varphi_0 = \pi/16$ agree with those ones obtained for straight nanowires [34].

If we look carefully, we will see that there are resonance modes that appear/disappear under certain parameters. To understand this phenomenon, we must keep in mind that the origin of the resonance mode, its frequency and amplitude are due to the interaction between the excitation field, corresponding to a *Sinc* pulse applied along the y-axis, with the magnetic moments present in the equilibrium state of the investigated systems. This means that maximum excitation occurs when the excitation field is perpendicular to the direction of the magnetic moments. For example, low-frequency modes 1 and 2, whose perturbations are mainly due to magnetic moments located at the edges of the nanotube, disappear when we have the case $\phi = 2\pi$ because the nanostructure no longer has the edges associated with these modes. Another special situation occurs with the disappearance of mode 3 when $\phi = \pi$. We must remember that this mode arises mainly from the ring-shaped magnetization patterns that form near the edges of the nanotube. As the magnetic moments in this position are parallel or antiparallel to the direction of the excitation field, their interaction is very weak, which causes the disappearance of this mode.

The analysis of Fig. 4 also reveals that the resonant modes are affected by the NT curvature. Indeed, two remarkable effects on the

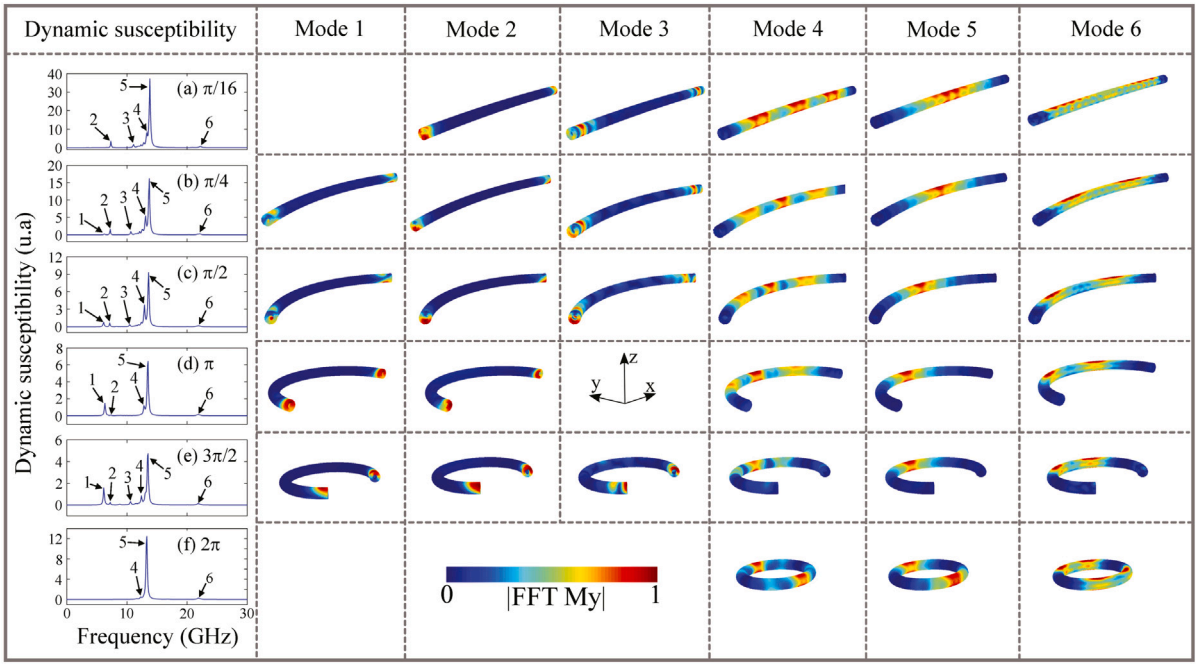

Fig. 4. Spatial profiles of the resonant modes shown in Fig. 3. The color scale of each panel corresponds to the amplitude of the magnetic moment fluctuations, with red depicting the largest amplitude and blue denoting zero amplitude. (For interpretation of the references to color in this figure legend, the reader is referred to the web version of this article.)

SWRM are the reduction of the amplitude of the dynamic susceptibility and the decrease in the area covered by the central mode peaks (modes 4, 5, and 6) as the curvature increases. These phenomena can be explained from the appearance of effective exchange-driven curvature-induced effective DMI and anisotropy [9]. Despite the model developed by Gaididei et al. [9] describes curved magnetic shells, it is a good approach to understand the curvature-induced effects we observed in the considered NTs. In this context, from parameterizing the normalized magnetization with a curvilinear basis ($\mathbf{r}_i$, θ, φ) as $\mathbf{m} = \mathbf{M}/M_s = \theta \sin\Theta\cos\Phi + \varphi \sin\Theta \sin\Phi + \mathbf{r}_i \cos\Theta$, and considering that the magnetization deviation from the in-surface state is represented by $\Theta = \pi/2 + \zeta$, the curvature-induced DMI energy density associated to these deviations is given by $\xi_D = -2A(\nabla\Theta \cdot \boldsymbol{\Gamma} + \nabla\Phi \cdot \boldsymbol{\Omega})$, where $\boldsymbol{\Gamma}$ is a vector depending on the surface's Gaussian and mean curvatures, and $\boldsymbol{\Omega}$ is the modified spin-connection. The expressions for $\boldsymbol{\Gamma}$ and $\boldsymbol{\Omega}$ for the geometry considered in this work have been previously obtained in Ref. [39]. The effective DMI accounts for determining the energetic cost to deviate the magnetic moments from a state given by constants Φ and Θ. If we assume the deviations from the in-surface state are very small ($\zeta \ll 1$), the exchange-driven curvature-induced DM energy is evaluated as

$$\xi_{\mathrm{D}} \approx 2A \frac{\partial\zeta}{\partial\varphi} \frac{\sin\theta}{\mathscr{L}^2}, \tag{2}$$

where $\mathscr{L} = R + r_e \sin\theta$, and terms of the order of ζ^2 have been neglected. Therefore, from Eq. (2) one can notice that the curvature-induced effective DMI depends on both the variation of ζ as a function of φ, and the NT curvature. Because this effective interaction penalizes the magnetic deviations from the in-surface direction originated from the spin wave excitations, the increase in the curvature (decrease in R) yields a decrease in the SWRM amplitudes. Additionally, the region where the magnetic moments point almost parallel to the surface increases. These results are in agreement with those obtained for the DS of toroidal nanorings with an onion-like ground state [31]. In this case one observes a decrease in the amplitude of the imaginary part of susceptibility as R increases. It is also worth notice that curvature-induced DMI effective interaction vanish for a straight NT ($R \to \infty$). Moreover, due to the absence of borders in a closed NT ($\varphi = 2\pi$), modes 1, 2, and 3 are not observed.

To complete our analysis, in Fig. 5 we summarize the behavior of the main characteristic resonance frequency observed in Figs. 3 and 4 as a function of thickness and curvature. In Fig. 5a, we present the frequency of the SWM as a function of β for different values of the opening angle φ_0. In all observed cases, the SW frequency decreases non-monotonically with the thickness of the NT. This decrease in the frequency as a function of the thickness for hollow nanomagnets is also observed in ferromagnetic nanospheres [26]. This behavior can be explained by the increase in the relation $\epsilon = E_m/E_x$ between magnetostatic E_m and exchange E_x contributions to the total energy [30]. Fig. 5b depicts the SW frequency as a function of φ_0 for different values of β. It can be observed that the frequency of the SWRM for mode 5 decreases quasi-linearly with the NT curvature. The decrease is more pronounced for thinner NTs due to their higher value of ϵ[30] and the consequent emergence of exchange-driven curvature-induced interactions in curved shells [9]. Comparing Figs. 5a and 5b we can conclude that a small curvature defined by $\phi = \pi/16$ generates a magnetic texture very similar to that of a straight wire.

Conclusions

Using micromagnetic simulations our study has shown that it is possible to tailor several features of spin-wave resonant modes in curved nanowires and nanotubes when a magnetic excitation is applied along the y-direction. Our results evidenced that it is possible to activate at least 5 characteristic resonant modes that correspond to magnetic moments in different regions of the nanostructure. In addition, it is possible to control the position of the main resonant mode of higher amplitude (mode 5, located at high frequencies) by varying the parameter β or the curvature of the system φ_0. The most interesting cases are observed when we fix the curvature (θ) and increase β. Therefore, by varying the geometry of the NW or NT we can tailor new resonant modes that can be useful for many applications that rely on spin-wave resonant modes.

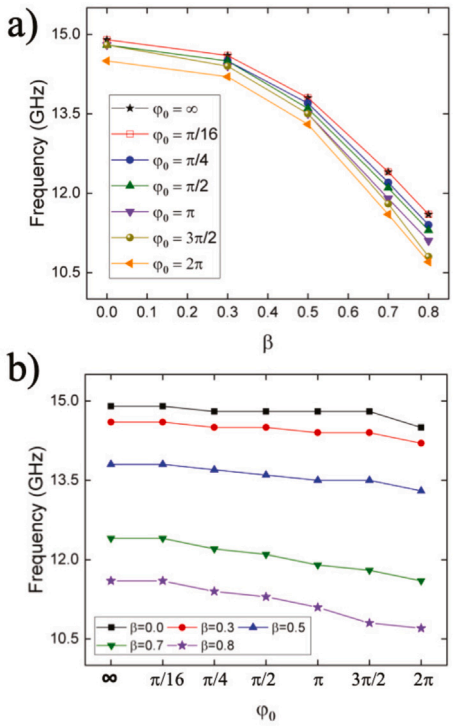

Fig. 5. Variation of evolution at resonance frequency with (a) ratio β at different values of φ_0 and (b) curvature dependent to poloidal angle φ_0 (toroidal parameter) for different values of β.

CRediT authorship contribution statement

E. Saavedra: Software, Investigation, Data curation. **S. Castillo-Sepúlveda:** Software, Validation, Investigation, Data curation. **R.M. Corona:** Software, Validation, Investigation, Data curation. **D. Altbir:** Resources, Writing – review & editing, Supervision, Funding acquisition. **J. Escrig:** Conceptualization, Resources, Writing – review & editing, Supervision, Visualization, Funding acquisition. **V.L. Carvalho-Santos:** Methodology, Formal analysis, Investigation, Data curation, Writing – original draft, Visualization.

Declaration of competing interest

The authors declare that they have no known competing financial interests or personal relationships that could have appeared to influence the work reported in this paper.

Acknowledgments

We acknowledge financial support from Financiamiento Basal para Centros Científicos *y* Tecnológicos under project AFB180001, Fondecyt 1200867 and 1200302.

Supplementary data

Supplementary material related to this article can be found online at https://doi.org/10.1016/j.rinp.2022.105290.

References

[1] Napoli G, Vergori L. Phys Rev Lett 2012;108:207803.
[2] Lapine M, Shadrivov IV, Powell DA, Kivshar YS. Nature Mater 2012;11:30.
[3] Georgiou T, Britnell L, Blake P, Gorbachev RV, Gholinia A, Geim AK, et al. Appl Phys Lett 2011;99:093103.
[4] Vedmedenko EY, Kawakami RK, Sheka DD, Gambardella P, Kirilyuk A, Hirohata A, et al. J Phys D: Appl Phys 2020;53:453001.
[5] Sheka DD. Appl Phys Lett 2021;118:230502.
[6] Streubel R, Tsymbal EY, Fischer P. J Appl Phys 2021;129:210902.
[7] Fernaández-Pacheco A, Streubel R, Fruchart O, Hertel R, Fischer P, Cowburn RP. Nat Comm 2017;8:15756.
[8] Streubel R, Lee J, Makarov D, Im M-Y, Karnaushenko D, Han L, et al. Adv Mater 2014;26:316.
[9] Gaididei Y, Kravchuk VP, Sheka DD. Phys Rev Lett 2014;112:257203.
[10] Yershov KV, Kravchuk VP, Sheka DD, Rößler UK. SciPost Phys 2020;9:043.
[11] Carvalho-Santos VL, Corona RM, Altbir D, Castillo-Sepúlveda S. Phys Rev B 2020;102:024444.
[12] Kravchuk VP, Sheka DD, Kákay A, Volkov OM, Rößler UK, van den Brink J, et al. Phys Rev Lett 2018;120:067201.
[13] Tejo F, Toneto D, Oyarzún S, Hermosilla J, Danna CS, Palma JL, et al. ACS Appl Mater Interfaces 2020;12:53454.
[14] Vojkovic S, Carvalho-Santos VL, Fonseca JM, Nuñez AS. J Appl Phys 2017;121:113906.
[15] Elías RG, Vidal-Silva N, Carvalho-Santos VL. Sci Rep 2019;9:14309.
[16] Pylypovskyi OV, Kononenko DY, Yershov KV, Rößler UK, Tomilo AV, Fassbender J, et al. Nano Lett 2020;20:8157.
[17] Espejo AP, Tejo F, Vidal-Silva N, Escrig J. Sci Rep 2017;7:4736.
[18] Allende S, Altbir D, Nielsch K. Phys Rev B 2009;80:174402.
[19] Toro OO, Alves SG, Carvalho-Santos VL, de Araújo CIL. J Appl Phys 2020;127:183905.
[20] Yershov KV, Kravchuk VP, Sheka DD, Gaididei Y. Phys Rev B 2015;92:104412.
[21] Skoric L, Donnelly C, Abert C, Hierro-Rodriguez A, Suess D, Fernández-Pacheco A. Appl Phys Lett 2021;118:242403.
[22] Moreno R, Carvalho-Santos VL, Espejo AP, Laroze D, Chubykalo-Fesenko O, Altbir D. Phys Rev B 2017;96:184401.
[23] Cacilhas R, de Araujo CIL, Carvalho-Santos VL, Moreno R, Chubykalo-Fesenko O, Altbir D. Phys Rev B 2020;101:184418.
[24] Yershov KV, Kravchuk VP, Sheka DD, Gaididei Y. Phys Rev B 2016;93:094418.
[25] Bittencourt GHR, Moreno R, Cacilhas R, Castillo-Sepúlveda S, Chubykalo-Fesenko O, Altbir D, et al. Appl Phys Lett 2021;118:142405.
[26] McKeever C, Ogrin FY, Aziz MM. J Appl Phys 2017;121:203901.
[27] Rana B, Kumar D, Barman S, Pal S, Mandal R, Fukuma Y, et al. J Appl Phys 2012;111:07, D503.
[28] Gubbiotti G, Xiong LL, Montoncello F, Adeyeye AO. Appl Phys Lett 2017;111:192403.
[29] Barman A, Mondal S, Sahoo S, De A. J Appl Phys 2020;128:170901.
[30] McKeever C, Ogrin FY, Aziz MM. Phys Rev B 2019;100:054425.
[31] XianYu Z-N, Du A. J Magn Magn Mater 2020;511:166955.
[32] Yoo Myoung-Woo, Lee Jae-Hyeok, Kim Sang-Koog. J Appl Phys 2014;116:223902.
[33] Abeed MA, Sahoo S, Winters D, Barman A, Bandyopadhyay S. Sci Rep 2019;9:16635.
[34] Saavedra E, Saez G, Díaz P, Cisternas E, Vogel EE, Escrig J. AIP Adv 2019;9:065007.
[35] Xiong LL, Adeyeye AO. Appl Phys Lett 2016;108:262401.
[36] Xiong LL, Kostylev M, Adeyeye AO. Phys Rev B 2017;95:224426.
[37] Saavedra E, Corona RM, Vidal-Silva N, Palma JL, Altbir D. J Escrig Sci Rep 2020;10:20024.
[38] Liu Q, Cao Q, Bi H, Liang C, Yuan K, She W, et al. Adv Mater 2016;28:486.
[39] Teixeira AW, Castillo-Sepúlveda S, Vojkovic S, Fonseca JM, Altbir D, Núñez ÁS, et al. J Magn Magn Mater 2019;478:253.
[40] Donahue MJ, Porter DG. OOMMF user's guide, version 1.2 a3. 2002, http://math.nist.gov/oommf.
[41] Dormand JR, Prince PJ. J Comput Appl Math 1980;6:19.
[42] Dormand JR, Prince PJ. J Comput Appl Math 1986;15:203.
[43] Willcox M, Ding A, Xu Y. 8th International vacuum electron sources conference and nanocarbon. IEEE; 2010, 11677496.
[44] Landau L, Lifshitz E. Phys Z Sowjetunion 1935;8:153.
[45] Gilbert TL. Phys Rev 1955;100:1243.
[46] Dao N, Donahue MJ, Dumitru I, Spinu L, Whittenburg SL, Lodder JC. Nanotechnology 2004;15:S634.
[47] Liu R, Wang J, Liu Q, Wang H, Jiang C. J Appl Phys 2008;103:013910.
[48] Wang Q, Jin L, Tang X, Bai F, Zhang H, Zhong Z. IEEE Trans Magn 2012;48:3246.
[49] Russek SE, Kaka S, Donahue MJ. J Appl Phys 2000;87:7070.
[50] Baker A, Beg M, Ashton G, Albert M, Chernyshenko D, Wang W, et al. J Magn Magn Mater 2017;421:428.
[51] Chernyshenko D. Computational methods in micromagnetics (Ph.D. thesis), University of Southampton; 2016.
[52] Brown Jr WF. Micromagnetics, Vol. 26. New York: Interscience Publishers; 1963.
[53] Han M, Guo W, Deng L. Sci China Technol Sci 2014;57:254–8.
[54] Luo J, et al. J Phys D: Appl Phys 2019;52:405001.

[55] Wen-Bing C, Man-Gui H, Hao Z, Yu O, Long-Jiang D. Chin Phys B 2010;19:087502.
[56] Talapatra A, Singh N, Adeyeye AO. Phys Rev Appl 2020;13:014034.
[57] Gerardin O, Youssef JB, Le Gall H, Vukadinovic N, Jacquart PM, Donahue MJ. J Appl Phys 2000;88:5899.
[58] Escrig J, Landeros P, Altbir D, Vogel EE, Vargas P. J Magn Magn Mater 2007;308:233.
[59] Mancilla-Almonacid D, Castro MA, Fonseca JM, Altbir D, Allende S, Carvalho-Santos VL. J Magn Magn Mater 2020;507:166754.
[60] Carvalho-Santos VL, Moura-Melo WA, Pereira AR. J Appl Phys 2010;108:094310.
[61] McMichael RD, Stiles MD. J Appl Phys 2005;97:10, J901.
[62] Kumar D, Dmytriiev O, Ponraj S, Barman A. J Phys D Appl Phys 2012;45:015001.